Mixing SABR models for Negative Rates

Alexandre Antonov, Michael Konikov, and Michael Spector
Numerix

August 9, 2015

Abstract

In the current low-interest-rate environment, extending option models to negative rates has become an important issue. In our previous paper, we introduced the Free SABR model, which is a natural and an attractive extension to the classical SABR model. In spite of its advantages over the Shifted SABR, the Free SABR option pricing formula is based on an approximation. Although this approximation is very good, it cannot guarantee the absence of arbitrage.

In this article, we build on an exact option pricing formula for the normal SABR with a free boundary and an arbitrary correlation. First, we derive this formula in terms of a 1D integral, which is suitable for fast calibration. Next, we apply the formula as a control variate to the Free SABR to improve the accuracy of its approximation, especially for high correlations. Finally, we come up with a Mixture SABR model, which is a weighted sum of the normal and free zero-correlation models. This model is guaranteed to be arbitrage free and has a closed-form solution for option prices. Added degrees of freedom also allow the Mixture SABR model to be calibrated to a broader set of trades, in particular, to a joint set of swaptions and CMS payment. We demonstrate this capability with a wide set of numerical examples.

1 Introduction

The SABR process with parameters $(F_0, v_0, \beta, \rho, \gamma)$[1] [6] for a rate F_t and its volatility v_t has the SDE

$$dF_t = F_t^\beta \, v_t \, dW_1, \tag{1}$$

$$dv_t = \gamma \, v_t \, dW_2, \tag{2}$$

with correlation $\mathbb{E}[dW_2 \, dW_1] = \rho dt$ and power $0 \le \beta < 1$. The solution is not uniquely defined by the SDE—we also need to impose some boundary conditions. The standard choice is to assume an absorbing boundary at zero, which enforces positivity and martingality conditions on the rate. See [1], [2], [5], [7], [9], [10], [13] for further references.

The SABR model is primarily used for volatility cube interpolation and for pricing CMS products by replication with vanilla options. It is also used in term-structure models, e.g., [12], [14].

At the time when the SABR model was introduced, positivity of the rates seemed like a reasonable and an attractive property. In current market conditions, where rates are extremely low and even negative, it

[1] Sometimes α is used instead of v_0.

is important to extend the SABR model to negative rates. For example, the Figure 1 displays historical evolution of the Swiss Franc (CHF) interest rates (overnight and Libors of tenors 1M, 3M, and 6M). We see that the rates drop negative, reaching as low as -2%. Another important observation is that the rates "stick" to zero for certain periods of time, suggesting their probability density functions have a singularity at zero.

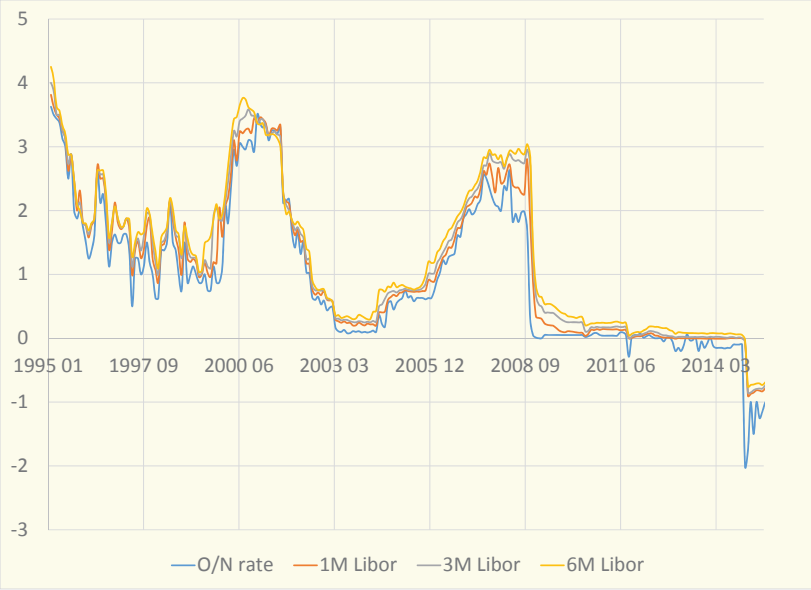

Figure 1: Swiss Franc interest rates.

The simplest way to take into account negative rates is to shift the SABR process to give an SDE of the form

$$dF_t = (F_t + s)^\beta \, v_t \, dW_1,$$

where s is a deterministic positive shift. This moves the lower bound on F_t from 0 to $-s$. One can either include the shift into calibration parameters $(v_0, \beta, \rho, \gamma, \mathbf{s})$ or fix it prior to calibration (e.g., to 2% in case of short rates of the Swiss Franc). Both ways have drawbacks.

Calibrating the shift does not really introduce a new degree of freedom—its influence on the skew is very similar to the power β, and may result in an identification problem. On the other hand, if one selects the shift value *manually* and calibrates only the standard parameters $(v_0, \beta, \rho, \gamma)$, there is always a danger that the rates can go lower than anticipated, and one will need to change this parameter accordingly. This can result in jumps in the other SABR parameters as the calibration response to such readjustment. As a consequence, there will be jumps in the values/Greeks of trades that are dependent on the swaption or cap volatilities. To cover for potential losses in such situations, traders are likely to be asked to reserve part of their P&L. Moreover, having the swaption prices being bounded from above (due to rate being bounded from below) can lead to situations when the shifted SABR cannot attain certain market prices. Therefore, we need a more natural and elegant solution to permit negative rates.

In [4], we introduced the Free SABR model

$$dF_t = |F_t|^\beta \, v_t \, dW_1$$

with $0 \le \beta < \frac{1}{2}$, and a *free* boundary. Such a model allows for negative rates and contains a certain "stickiness" at zero. Moreover, the model satisfies norm-preserving and martingale requirements.

We calculated the exact option price for the *zero-correlation* case and came up with an accurate approximation for general correlations. However, the approximation accuracy can degenerate in some cases (especially those related to large strikes and high correlation).

In this article, we build on the normal SABR to improve the approximation accuracy of the Free SABR. An analytical solution for the normal SABR with a free boundary,

$$dF_t = v_t \, dW_1,$$

appeared first in [11] in the form of a 2D integral. Below, we present an equivalent 1D integral formula, where the integrand can be approximated with very high accuracy in closed form. This way, the model becomes feasible for calibration purposes. First, we use the normal SABR to improve the accuracy of the Free SABR approximation for rare problematic cases. Second, we construct a new model as a *mixture* of the normal SABR and the zero-correlation Free SABR. Importantly, *this model is arbitrage free and does not require any approximation in the option-pricing formula*. Moreover, it contains more parameters to ensure an accurate calibration to swaptions and CMS payments. In the numerical experiments section, we demonstrate the superiority of the Mixture SABR calibration over the Shifted and Free SABR models.

In what follows, we consider only the $F_0 > 0$ case (unless explicitly stated otherwise). When $F_0 < 0$, we note that $\tilde{F}_t = -F_t$ satisfies the SABR SDE with parameters $(-F_0, v_0, \beta, -\rho, \gamma)$, and the *time value* of a European option (call or put) on F_t struck at K equals that of an option on $\tilde{F}_t$ struck at $-K$. We do not distinguish between call and put *time values* because, for norm-preserving martingale processes, $\mathbb{E}[(F_T - K)^+] - (F_0 - K)^+ = \mathbb{E}[(K - F_T)^+] - (K - F_0)^+$.

The article is organized as follows. First, we briefly review the Free SABR model and its option pricing formula derived in [4]. Then we introduce the Normal Free SABR and our new option pricing formula for this model. We follow with the two main uses of the Normal Free SABR: as a control variate to improve accuracy of the general Free SABR model in the tails, and as a component of the new model we propose. This new model is a mixture of two SABR models that is guaranteed to be arbitrage free and still allows for a closed-form solution for option prices. Finally, we compare all three models—the Shifted SABR, the Free SABR, and the Mixture SABR—in how well they can calibrate to swaptions only and to combinations of swaptions and a single CMS payment.

2 Free-boundary SABR

We briefly review the main properties of the *free*-boundary SABR (or Free SABR)

$$dF_t = |F_t|^\beta \, v_t \, dW_1, \tag{3}$$

$$dv_t = \gamma \, v_t \, dW_2, \tag{4}$$

for $0 \le \beta < \frac{1}{2}$. Such a construction permits negative rates, and the rates exhibit a "stickiness" at zero. Details can be found in [4].

The zero-correlation Free SABR model can be solved exactly: the option time value can be written as

$$\mathcal{O}_F(T,K) = \mathbb{E}\left[(F_T-K)^+\right] - (F_0-K)^+ = \frac{1}{\pi}\sqrt{|KF_0|}\left\{\mathbf{1}_{K\geq 0}A_1 + \sin(|\nu|\,\pi)\,A_2\right\} \tag{5}$$

with integrals

$$A_1 = \int_0^\pi d\phi \frac{\sin\phi \sin\left(|\nu|\,\phi\right)}{b-\cos\phi}\,\frac{G(T\,\gamma^2, s(\phi))}{\cosh s(\phi)}, \tag{6}$$

$$A_2 = \int_0^\infty d\psi \frac{\sinh\psi\left(\mathbf{1}_{K\geq 0}\cosh(|\nu|\,\psi) + \mathbf{1}_{K<0}\sinh(|\nu|\,\psi)\right)}{b+\cosh\psi}\,\frac{G(T\,\gamma^2, s(\psi))}{\cosh s(\psi)}, \tag{7}$$

where $\nu = -\frac{1}{2(1-\beta)}$ and

$$b = \frac{|F_0|^{2(1-\beta)} + |K|^{2(1-\beta)}}{2\,|F_0\,K|^{1-\beta}}.$$

Here s has the following parameterizations with respect to ϕ and ψ:

$$\sinh s(\phi) = \gamma\, v_0^{-1}\,\sqrt{2\bar{q}(b-\cos\phi)} \quad \text{and} \quad \sinh s(\psi) = \gamma\, v_0^{-1}\,\sqrt{2\bar{q}(b+\cosh\psi)},$$

where $\bar{q} = \frac{|F_0\,K|^{1-\beta}}{(1-\beta)^2}$.

The function

$$G(t,s) = 2\sqrt{2}\frac{e^{-\frac{t}{8}}}{t\sqrt{2\pi t}}\int_s^\infty du\, u\, e^{-\frac{u^2}{2t}}\sqrt{\cosh u - \cosh s}$$

has been introduced in [2]. It is closely related to the McKean heat kernel on the hyperbolic plane H^2. It is important to notice that, although the function $G(t,s)$ is a 1D integral, it can be *very* efficiently approximated by a closed formula (see [2]).

Let us pass now to a *general correlation* option time value

$$\mathcal{O}_F(T,\,K;\,v_0,\beta,\rho,\gamma) = \mathbb{E}\left[(F_T-K)^+\right] - (F_0-K)^+\,, \tag{8}$$

where we have explicitly restored the SABR parameters. There is no closed form for the general case, so we approximate it using the zero-correlation Free SABR model (also called *mimicking* model)

$$d\tilde{F}_t = |\tilde{F}|_t^{\tilde{\beta}}\,\tilde{v}_t\,d\tilde{W}_1 \quad \text{and} \quad d\tilde{v}_t = \tilde{\gamma}\,\tilde{v}_t\,d\tilde{W}_2,$$

with $\mathbb{E}[d\tilde{W}_1\,d\tilde{W}_2] = 0$ and specially calculated coefficients $\{\tilde{v}_0, \tilde{\beta}, \tilde{\gamma}\}$. The power and vol-of-vol are strike-independent:

$$\tilde{\beta} = \beta \quad \text{and} \quad \tilde{\gamma}^2 = \gamma^2 - \frac{3}{2}\left\{\gamma^2\rho^2 + v_0\gamma\rho\,(1-\beta)\,F_0^{\beta-1}\right\}.$$

The initial stochastic volatility is more complicated and *strike-dependent*; its expansion $\tilde{v}_0 = \tilde{v}_0^{(0)} + T\,\tilde{v}_0^{(1)} + \cdots$ can be found in [4]. The option time value

$$\tilde{\mathcal{O}}_F(T,\,K;\,v_0,\beta,\rho,\gamma) \equiv \mathcal{O}_F(T,\,K;\,\tilde{v}_0,\beta,0,\tilde{\gamma}), \tag{9}$$

which is calculated using the closed form (5), is a good approximation of our general case:

$$\mathcal{O}_F(T,\,K;\,v_0,\beta,\rho,\gamma) \simeq \tilde{\mathcal{O}}_F(T,\,K;\,v_0,\beta,\rho,\gamma).$$

Below we briefly address behavior of the Free SABR call option $\mathcal{C}_F^{\rm SABR}(T,K)$ for sensitive limiting cases. Similar to the CEV model, the Free SABR call price is a smooth function of the strike and forward. Indeed, one can show that

$$\begin{aligned}\mathcal{C}_F &\underset{K\to 0}{=} C_1 + C_2\,K + C_3\,|K|^{2(1-\beta)} + \cdots\,,\\ \mathcal{C}_F &\underset{F_0\to 0}{=} C_1' + C_2'\,F_0 + C_3'\,|F_0|^{2(1-\beta)} + \cdots\,,\end{aligned}$$

where the constants C_i and C_i' depend on the model parameters. This means that call option "delta" is a smooth function of F_0 with the following behavior around zero:

$$\partial\mathcal{C}_F^{\rm SABR}/\partial F_0 \underset{F_0\to 0}{=} C_2' + C_3'\,2(1-\beta)\,{\rm sign}(F_0)\,|F_0|^{1-2\beta} + \cdots\,.$$

The option "gamma" is smooth everywhere except zero. This weak (integrable) divergence around zero, $\partial^2\mathcal{C}_F^{\rm SABR}/\partial F_0^2 \sim |F_0|^{-2\beta}$, reflects the "stickiness" of the rate. On the other hand, standard Greek calculations (using finite differences with 1–5 bps spacing) produce a moderate, finite "gamma" spike at zero.

We have mentioned in [4] that the CEV model for the zero spot case has a symmetric density function and, consequently, has zero implied volatility skew at zero strike. This property is also valid for the zero-correlation Free SABR. However, for the general Free SABR model, the asymmetry is introduced by the correlation with the stochastic volatility. This means that, for small or zero spot values, the model can control the normal implied volatility skew around zero strikes by means of the correlation.

The case $\beta = 0$ is clearly regular: it corresponds to the normal Free SABR. Looking forward, we note that its option price is analytical function of the strike and forward at zero: all Greeks exist and are finite for $F_0 = 0$ and $K = 0$. Moreover, there exists an exact formula for the normal Free SABR model for any correlation.

3 Normal free-boundary SABR

It turns out that if we consider the case of normal SABR with free boundary, i.e.,

$$dF_t = v_t\,dW_1, \tag{10}$$
$$dv_t = \gamma\,v_t\,dW_2, \tag{11}$$

with some correlation $E[dW_2\,dW_1] = \rho dt$, it is possible to derive a closed-form solution for a call option value even if correlation is not zero:

$$\mathcal{O}_N(T,K) = \mathbb{E}\left[(F_T-K)^+\right] - (F_0-K)^+ = \frac{V_0}{\pi}\int_{s_0}^{\infty}\frac{G(\gamma^2T,s)}{\sinh s}\sqrt{\sinh^2 s - (k-\rho\cosh s)^2}ds, \tag{12}$$

where

$$\begin{aligned}\cosh s_0 &= \frac{-\rho k + \sqrt{k^2 + \bar{\rho}^2}}{\bar{\rho}^2},\\ k &= \frac{K - F_0}{V_0} + \rho,\\ V_0 &= \frac{v_0}{\gamma},\\ \bar{\rho} &= \sqrt{1-\rho^2}.\end{aligned} \tag{13}$$

The proof of this formula and its comparison with [11] is given in Appendix A. We note that the option pricing formula appeared first in [11] as a *2D* integral. Below, we present an equivalent 1D integral formula where the integrand can be approximated with very high accuracy in a closed form. This way, the model becomes feasible for calibration purposes.

It is easy to see that the option price is a regular function of spot and strike even when their values are zero: all the derivatives with respect to spot and strike are finite. The normal SABR behavior at zero is not "sticky".

4 Improving the Free SABR accuracy by a control variate

The Normal Free SABR can serve as a control variate for a general Free SABR. Suppose we use a Free SABR model with parameters $(v_0, \beta, \rho, \gamma)$ to price an option for which exact the analytical solution $\mathcal{O}_F(T,\, K;\, v_0, \beta, \rho, \gamma)$ is not known. Instead we use the mimicking approximation (9),

$$\mathcal{O}_F(T,\, K;\, v_0, \beta, \rho, \gamma) \simeq \tilde{\mathcal{O}}_F(T,\, K;\, v_0, \beta, \rho, \gamma),$$

which becomes exact for $\rho = 0$.

To apply the control variate technique, we choose a normal SABR model that best resembles the original one. We keep the correlation between factors the same and choose the normal v_0 parameter to roughly preserve the ATM normal volatility. We adjust the approximation (9) by adding on a control variate term:

$$\mathcal{O}_F(T,\, K;\, v_0, \beta, \rho, \gamma) \simeq \tilde{\mathcal{O}}_F(T,\, K;\, v_0, \beta, \rho, \gamma) + \left\{\mathcal{O}_N(T, K; v_0 F_0^{\beta}, \rho, \gamma) - \tilde{\mathcal{O}}_F(T, K; v_0 F_0^{\beta}, 0, \rho, \gamma)\right\}, \tag{14}$$

where $\mathcal{O}_N(T, K; v_0 F_0^{\beta}, \rho, \gamma)$ stands for the exact normal SABR option time value (12). This adjusted formula is exact when for both the $\rho = 0$ and $\beta = 0$ cases. For values in between, the error coming from the inexactness of the mapping methodology will be partially canceled between the general and the zero-β values. We demonstrate this accuracy gain in the numerical experiments.

5 Mixture SABR

Another approach that uses a closed-form solution for the normal SABR with arbitrary correlation is a mixture approach. Instead of mapping a nonzero correlation SABR into a zero-correlation one, we can *define* our model as a mixture of a zero-correlation SABR and a normal SABR. Assume the forward rate F_t can be written as

$$F_t = \chi F_t^{(1)} + (1-\chi) F_t^{(2)},$$

where

- $F_t^{(1)}$ follows a *zero-correlation* Free SABR model with parameters (α_1, β_1, 0, γ_1),
- $F_t^{(2)}$ follows a *normal* Free SABR model with parameters (α_2, 0, ρ_2, γ_2),
- χ is a random variable taking value 1 with probability p and 0 with probability $1-p$ and independent of both SABR processes.

Clearly, this model is arbitrage-free and permits negative rates.

Moreover, both of these component models have closed-form solutions for option values, and, consequently, so does the mixture model. In addition, we get some extra degrees of freedom, which could be used for either calibration to a larger number of options or for a joint calibration to swaptions and CMS quotes. We verify the latter with numerical experiments in Section 7.

Let us comment now on the parameter choices for the Mixture SABR. It is always useful to keep the same ATM volatility for both models, leading to the following relation of the initial stochastic volatility:

$$\sigma_0 = \alpha_1 F_0^{\beta_1} = \alpha_2. \tag{15}$$

The other parameters can be independent for greater calibration freedom.

A useful parametrization of the probability as a function of a parameter s is

$$p(s) = \frac{\sigma_0\,\beta_1\,e^s}{\sigma_0\,\beta_1\,e^s + |\gamma_2\,\rho_2|}, \tag{16}$$

which guarantees the Mixture SABR model degeneration to either zero-correlation or normal SABR when $\rho_2 = 0$ or $\beta_1 = 0$, respectively.

The probability parameter can be also used to control the singularity at zero. Namely, excluding it from the calibration parameters and setting it to small value reduces the singularity arising from the zero-correlation model. We recommend, however, using the parametrization (16) for calibration, because the singularity is indeed observed in the rates time series (Figure 1).

Parameter intuition. Both models (the zero-correlation SABR and the Normal SABR) yield the same ATM volatility (because of the constraint (15)), so the Mixture SABR will have the same ATM volatility as well.

The zero-correlation model influences the smile skew with its power β_1 while the normal one works with the smile skew with its correlation. The mixture of these models weights the above skew behaviors.

The vol-of-vols of the component models $\{\gamma_1, \gamma_2\}$ influences both the smile curvature and the edges. We recall that the asymptotics of a SABR model for large strikes can be presented in terms of its the Black-Scholes volatility tending to

$$\sigma_{BS}(K)\Big|_{K\to\infty} = \frac{\gamma}{1-\beta}; \tag{17}$$

see [2] and references where-in. Thus, the Mixture model, having one γ-parameter more than the Shifted and the Free SABR models, can *detach* the smile curvature and the edges. As we will see later, this feature permits the Mixture SABR to calibrate to both swaptions and CMS quotes.

Reduced parametrization. There is also a *reduced parametrization* set where we impose the constraints

$$\begin{aligned} \gamma_2 &= \frac{\gamma_1}{1-\beta_1}, \\ p &= \frac{\sigma_0\,\beta_1}{\sigma_0\,\beta_1 + |\gamma_2\,\rho_2|}. \end{aligned} \tag{18}$$

The first constraint links the vol-of-vols to keep the same asymptotics for both models for large strikes (17). The second constraint corresponds to $s = 0$ in the probability parametrization (16), which allows us to recover the pure zero-correlation or normal cases and keeps approximately the same skew around the ATM strikes. The reduced parametrization restores the same number of parameters (and their approximate meaning in terms of the volatility surface) as in the Free SABR case.

6 Comparing the Shifted, Free, and Mixture SABR models

In this section, we compare the Shifted, Free and Mixture SABR models. As already discussed, the Shifted SABR has a shift parameter which is not calibrated to the implied market information, but is manually set instead. New information about the spot rate can eventually invalidate the shift. For example, if the rate falls down to -2.2%, a shift of 2% will no longer be compatible with the market. This means that we should reset the shift and recalibrate the model. This will produce a jump in *all* volatility sensitive instruments.

The Free and Mixture SABR models are free of this behavior—their parameters are either calibrated or set without any future incompatibility with the market.

The analytical formulae for the Shifted and the Free SABR models are approximations. Their quality is, in general, good, but it can deteriorate in some cases, especially in the wings of the distribution. Sometimes, an ad-hoc adjustment is necessary. On the other hand, the Mixture SABR analytics is exact and free of such (sometimes painful) adjustments.

We should also mention that all three models can be calibrated to observed swaption quotes. However, the Shifted and the Free SABR models have too few parameters to attempt a joint calibration to swaptions and CMS quotes. Indeed, they lack extra parameters to control the behaviors of the wings. The Mixture SABR has more degrees of freedom and is suitable for such a joint calibration. We address these points in the numerical experiments section below.

Finally, the Free and Mixture SABR models have a singularity at zero which corresponds to the "stickiness" of rate process at zero, which is observed in the historical rates data. Having said that, one can attenuate this singularity by decreasing the probability in the Mixture SABR if desired.

7 Numerical experiments

We perform a number of numerical experiments to show the advantage of the Mixture SABR model. Not only do we see improved accuracy when calibrating to swaptions, but the Mixture SABR model handles the joint calibration problem as well.

7.1 Effect of control variate

We analyze the *normal implied volatility* (bps) for European call options $\mathcal{C}(T,K) = E[(F_T - K)^+]$ for the free-boundary SABR with the parameters shown in Table 1. The results are shown in Tables 2 and 2. The "Exact" column shows the results obtained with a high quality Monte Carlo simulation described in [4]. The "Adjusted" and "Unadjusted" columns show the results obtained with our formula for the Free SABR with and without the control variate respectively. The bold line ($K = 1$) represents the ATM strike.

Parameter	**Symbol**	**Value for Input I**	**Value for Input II**
Rate Initial Value	F_0	50 bps	1%
SV Initial Value	v_0	$0.6\,F_0^{1-\beta}$	$0.3\,F_0^{1-\beta}$
Vol-of-Vol	γ	0.3	0.3
Correlations	ρ	-0.3	-0.3
Skews	β	0.25	0.25
Maturities	T	3Y	10Y

Table 1: Setups for the free-boundary SABR model.

K	**Unadjust**	**Adjusted**	**Exact**	**Unadj − Exact**	**Adj − Exact**
-0.8	29.83	29.78	29.95	-0.12	-0.17
-0.65	28.79	28.85	28.97	-0.18	-0.12
-0.5	27.79	27.91	27.99	-0.20	-0.08
-0.35	26.82	26.99	27.04	-0.22	-0.05
-0.2	25.95	26.12	26.15	-0.20	-0.03
-0.05	25.30	25.43	25.46	-0.16	-0.03
0.1	25.77	25.84	25.85	-0.08	-0.01
0.25	26.62	26.69	26.69	-0.07	0.00
0.4	27.33	27.39	27.39	-0.06	0.00
0.55	27.90	27.96	27.97	-0.07	-0.01
0.7	28.38	28.44	28.45	-0.07	-0.01
0.85	28.80	28.85	28.87	-0.07	-0.02
1	**29.17**	**29.23**	**29.25**	**-0.08**	**-0.02**
1.15	29.53	29.58	29.60	-0.07	-0.02
1.3	29.87	29.92	29.94	-0.07	-0.02
1.45	30.22	30.26	30.29	-0.07	-0.03
1.6	30.57	30.61	30.63	-0.06	-0.02
1.75	30.94	30.97	30.99	-0.05	-0.02
1.9	31.33	31.36	31.37	-0.04	-0.01

Table 2: Results for input I. The bold line represents the ATM strike.

K	Unadjust	Adjusted	Exact	Unadj – Exact	Adj – Exact
-0.8	38.43	39.06	39.24	-0.81	-0.18
-0.65	36.80	37.44	37.60	-0.80	-0.16
-0.5	35.18	35.82	35.97	-0.79	-0.15
-0.35	33.59	34.19	34.33	-0.74	-0.14
-0.2	32.05	32.60	32.73	-0.68	-0.13
-0.05	30.67	31.12	31.25	-0.58	-0.13
0.1	30.20	30.51	30.63	-0.43	-0.12
0.25	30.18	30.49	30.51	-0.33	-0.02
0.4	30.13	30.43	30.41	-0.28	0.02
0.55	30.06	30.35	30.31	-0.25	0.04
0.7	29.99	30.27	30.22	-0.23	0.05
0.85	29.98	30.23	30.18	-0.20	0.05
1	**30.05**	**30.27**	**30.22**	**-0.17**	**0.05**
1.15	30.24	30.42	30.36	-0.12	0.06
1.3	30.56	30.69	30.63	-0.07	0.06
1.45	31.03	31.09	31.04	-0.01	0.05
1.6	31.63	31.64	31.58	0.05	0.06
1.75	32.35	32.31	32.26	0.09	0.05
1.9	33.17	33.10	33.04	0.13	0.06

Table 3: Results for input II. The bold line represents the ATM strike.

We observe that the adjusted model displays better accuracy, especially in the wings.

7.2 Calibration to swaptions

In this section we consider real data from July 1, 2015 for a Swiss Franc 1Y4 swaption with a negative forward rate of -11 bps. The input is presented Table 4 in terms of normal implied volatility in pairs of strike & volatility, $\{K_i, \sigma_i\}$.

Strike (%)	Vol (bps)
-0.3	56.42
-0.11	57.08
0.14	64.2
0.39	71.31
0.89	85.55
1.89	114.32

Table 4: Swaption 1Y4 calibration input: strike vs. implied normal volatility.

We calibrate our SABR models (Shifted, Free and Mixture) to this data. The Mixture model is calibrated either in the reduced form (18) or in the full one. We note that the ATM volatilities are always linked together (15). The calibrated parameters are presented in Table 5.

Shifted		Free		Mixture		
					Reduced	Full
α	0.0058	α	0.0072	α_1	0.0183	0.0333
β	0.0121	β	0.0380	β_1	0.1720	0.2589
γ	1.0375	γ	0.9029	γ_1	0.7372	0.0150
ρ	0.4136	ρ	0.5350	α_2	0.0057	0.0057
shift	0.0200			ρ_2	0.9845	0.6187
				γ_2	0.8904	0.9861
				p	0.5035	0.2396

Table 5: Calibrated parameters for the Shifted, Free, and Mixture SABR models calibrating to the data in Table 4.

Table 6 indicates that the calibration accuracy is very good for all models. (The largest error is around 1 bp.) Table 7 shows the comparison of the analytical approximation with the exact solution for the Shifted and Free SABR models. We observe high approximation accuracy.

Strike (%)	Target (bps)	Shifted (bps)	Free(bps)	Mixture (bps)	
				Reduced	Full
-0.3	56.42	55.81	55.71	56.00	56.02
-0.11	57.08	58.28	58.54	58.18	58.12
0.14	64.20	63.90	63.63	63.48	63.60
0.39	71.31	70.83	70.99	70.99	71.01
0.89	85.55	85.63	85.70	86.02	85.82
1.89	114.32	114.41	114.27	114.22	114.31

Table 6: Calibration accuracy for Shifted, Free, and Mixture SABR models.

Strike (%)	Shifted (bps)			Free (bps)		
	Analyt	Exact	Diff	Analyt	Exact	Diff
-0.3	55.81	55.48	0.33	55.71	55.70	0.01
-0.11	58.28	58.11	0.16	58.54	58.73	-0.19
0.14	63.90	63.99	-0.08	63.63	65.05	-1.41
0.39	70.83	71.05	-0.22	70.99	72.52	-1.52
0.89	85.63	86.01	-0.38	85.70	87.57	-1.87
1.89	114.41	115.02	-0.62	114.27	115.92	-1.65

Table 7: Approximation accuracy of the closed-form approximation. The "exact" data is computed with a high-accuracy Monte Carlo method.

7.3 Joint calibration to swaptions and CMS payment

In this section, we consider a more challenging calibration setup where we calibrate to both the swaptions from Table 4 and a CMS payment.

We recall that the CMS convexity adjustment depends on the variance of the rate process, which can be evaluated by the usual static replication formula [8]:

$$\mathbb{V}[F_T] \equiv \mathbb{E}[F_T^2] - F_0^2 = 2\int_{-\infty}^{\infty} dK\, \mathcal{O}(T,K). \tag{19}$$

As usual, $\mathcal{O}(T,K)$ is an option time value.

Unfortunately, CMS quotes are not always available in the market for a given swap rate. In this article, we analyze the ability of the Shifted, Free, and Mixture SABR models to reach different CMS prices. We will quote the CMS payment in terms of its normal implied volatility σ_{CMS}, i.e.,

$$\mathbb{E}\left[F_T^2\right] - F_0^2 = T\sigma_{\text{CMS}}^2 \tag{20}$$

Let us determine a *minimal* volatility σ_{CMS} compatible with the input $\{K_i,\, \sigma_i\}_{i=1}^N$ from Table 4. We start with constructing a curve of the implied volatility $\sigma(K)$ by using linear interpolation, between the market nodes $\sigma(K_i) = \sigma_i$. Next we integrate the r.h.s. of (19) from the first quoted strike to the last one using the Bachelier formula for the option price:

$$\mathcal{O}(T,K) = \mathcal{O}_B(T,K,\sigma) \equiv \mathbb{E}\left[(F_0 - K + \sigma\sqrt{T}\,Z)^+\right] - (F_0 - K)^+, \tag{21}$$

where Z is a standard Gaussian variable with zero mean and unit variance. The minimal CMS volatility, found by

$$T\tilde{\sigma}_{\text{CMS}}^2 = 2\int_{K_1}^{K_N} dK\, \mathcal{O}_B(T,K,\sigma(K)) \tag{22}$$

with the input data in Table 4, will be around sixty bps,

$$\tilde{\sigma}_{\text{CMS}} \simeq 60 \text{ bps}.$$

Other interpolations, e.g., SABR ones, do not change the answer dramatically, so we can state that the CMS payment with a smaller volatility is *incompatible* with the swaptions input.

In our experiments, we examine a joint calibration to the set of swaptions and CMS volatilities from 50 bps to 100 bps, and analyze the results for all models: Shifted, Free, and Reduced Mixture and (full) Mixture.

In Tables 8–11, we show the swaption and CMS volatilities from the jointly calibrated models for the range of input CMS volatilities and swaption strikes. We also include RMS error in the calibrated values.[2] The swaption volatilities in bold correspond to the quoted strikes while the normal font volatilities represent the distribution edges. The calibrated values of the models are shown in Appendix B.

Input CMS vol (bps)	50	60	70	80	90	100
Calibrated CMS vol (bps)	64.22	66.26	70.81	77.13	84.81	91.85
Strike (%)						
-1.5	19.70	30.99	58.96	73.46	80.70	82.50
-1	24.23	33.47	54.58	66.88	73.67	74.91
-0.5	43.23	45.78	53.18	59.33	62.92	62.72
-0.3	**50.04**	**51.81**	**55.07**	**57.97**	**59.44**	**58.48**
-0.11	**56.10**	**57.50**	**58.35**	**58.75**	**58.35**	**57.09**
0.14	**63.62**	**64.81**	**64.21**	**63.07**	**61.75**	**61.31**
0.39	**70.75**	**71.90**	**70.98**	**69.75**	**68.87**	**69.52**
0.89	**84.13**	**85.44**	**85.36**	**85.48**	**86.27**	**88.61**
1.89	**108.62**	**110.61**	**113.91**	**117.59**	**121.68**	**126.47**
2	111.18	113.26	116.97	121.04	125.48	130.49
3	133.58	136.51	144.05	151.56	158.99	166.00
RMS Error (bps)	6.31	3.28	0.79	1.99	3.86	5.85

Table 8: Shifted SABR joint calibration output. The calibrated swaption volatilities are expressed in bps.

[2]Explicitly, the RMS error is $\sqrt{\frac{\left(\sigma^{(C)}_{\rm CMS}-\sigma_{\rm CMS}\right)^2+\sum_{i=1}^{N}\left(\sigma^{(C)}_i-\sigma_i\right)^2}{N+1}}$, where the volatilities with the superscript (C) correspond to the *calibrated* values.

Input CMS vol (bps)	50	60	70	80	90	100
Calibrated CMS vol (bps)	64.25	66.46	70.78	78.55	88.19	95.33
Strike (%)						
-1.5	31.87	42.20	40.04	55.83	69.73	76.79
-1	30.01	38.89	38.85	53.54	63.20	68.51
-0.5	42.47	45.91	47.73	53.87	58.88	62.38
-0.3	**49.32**	**51.54**	**54.06**	**57.85**	**60.43**	**62.79**
-0.11	**55.58**	**57.18**	**58.78**	**60.02**	**59.94**	**60.64**
0.14	**63.38**	**64.57**	**63.72**	**62.23**	**60.02**	**59.23**
0.39	**70.76**	**71.84**	**72.06**	**70.71**	**68.97**	**68.71**
0.89	**84.53**	**85.65**	**86.70**	**85.60**	**84.77**	**85.19**
1.89	**109.42**	**110.97**	**112.69**	**113.32**	**115.84**	**117.94**
2	112.00	113.62	115.42	116.35	119.36	121.68
3	134.47	136.70	139.50	144.52	152.52	156.89
RMS Error (bps)	6.35	3.32	1.41	1.60	2.76	4.14

Table 9: Free SABR joint calibration output. The calibrated swaption volatilities are expressed in bps.

Input CMS vol (bps)	50	60	70	80	90	100
Calibrated CMS vol (bps)	64.11	66.61	71.03	77.80	84.57	93.59
Strike (%)						
-1.5	39.49	46.77	67.87	88.35	99.35	112.41
-1	28.68	42.44	58.41	73.19	82.27	92.65
-0.5	42.65	47.05	53.59	58.65	65.27	73.22
-0.3	**49.79**	**51.97**	**54.91**	**58.03**	**61.55**	**65.65**
-0.11	**56.07**	**57.27**	**58.12**	**58.10**	**57.80**	**57.16**
0.14	**63.78**	**64.48**	**64.18**	**62.48**	**60.59**	**57.86**
0.39	**71.00**	**71.63**	**71.15**	**70.69**	**70.19**	**68.97**
0.89	**84.41**	**85.39**	**85.64**	**86.69**	**87.87**	**88.29**
1.89	**108.55**	**110.85**	**113.62**	**115.86**	**118.64**	**120.46**
2	111.06	113.51	116.58	118.89	121.78	123.69
3	132.81	136.76	142.54	145.30	148.90	151.20
RMS Error (bps)	6.31	3.29	0.84	1.49	3.68	5.57

Table 10: Reduced mixture SABR joint calibration output. The calibrated swaption volatilities are expressed in bps.

Input CMS vol (bps)	50	60	70	80	90	100
Calibrated CMS vol (bps)	64.05	66.55	70.96	80.03	89.95	99.86
Strike (%)						
-1.5	37.16	47.30	66.85	84.63	82.44	82.54
-1	28.95	41.99	58.01	64.80	60.34	59.59
-0.5	42.37	46.42	53.48	54.27	53.97	53.80
-0.3	**49.73**	**52.03**	**55.21**	**56.02**	**56.20**	**56.17**
-0.11	**56.10**	**57.53**	**58.07**	**58.07**	**57.98**	**58.21**
0.14	**63.84**	**64.57**	**63.89**	**63.50**	**63.41**	**63.64**
0.39	**71.05**	**71.40**	**71.16**	**71.16**	**71.28**	**71.09**
0.89	**84.43**	**84.86**	**85.64**	**85.88**	**85.74**	**85.13**
1.89	**108.51**	**111.11**	**113.71**	**114.22**	**114.35**	**114.89**
2	111.01	113.87	116.73	117.33	117.64	118.45
3	132.68	137.83	143.39	145.72	149.09	153.30
RMS Error (bps)	6.31	3.23	0.74	0.50	0.47	0.56

Table 11: Mixture SABR joint calibration output. The calibrated swaption volatilities are expressed in bps.

Table 12 shows the calibration errors for each model.

Input CMS vol (bps)		50	60	70	80	90	100
Model	**Strike (%)**						
Shifted	-0.3	-6.38	-4.61	-1.35	1.55	3.02	2.06
	-0.11	-0.98	0.42	1.27	1.67	1.27	0.01
	0.14	-0.58	0.61	0.01	-1.13	-2.45	-2.89
	0.39	-0.56	0.59	-0.33	-1.56	-2.44	-1.79
	0.89	-1.42	-0.11	-0.19	-0.07	0.72	3.06
	1.89	-5.70	-3.71	-0.41	3.27	7.36	12.15
Free	-0.3	-7.10	-4.88	-2.36	1.43	4.01	6.37
	-0.11	-1.50	0.10	1.70	2.94	2.86	3.56
	0.14	-0.82	0.37	-0.48	-1.97	-4.18	-4.97
	0.39	-0.55	0.53	0.75	-0.60	-2.34	-2.60
	0.89	-1.02	0.10	1.15	0.05	-0.78	-0.36
	1.89	-4.90	-3.35	-1.63	-1.00	1.52	3.62
Reduced Mixture	-0.3	-6.63	-4.45	-1.51	1.61	5.13	9.23
	-0.11	-1.01	0.19	1.04	1.02	0.72	0.08
	0.14	-0.42	0.28	-0.02	-1.72	-3.61	-6.34
	0.39	-0.31	0.32	-0.16	-0.62	-1.12	-2.34
	0.89	-1.14	-0.16	0.09	1.14	2.32	2.74
	1.89	-5.77	-3.47	-0.70	1.54	4.32	6.14
Mixture	-0.3	-6.69	-4.39	-1.21	-0.40	-0.22	-0.25
	-0.11	-0.98	0.45	0.99	0.99	0.90	1.13
	0.14	-0.36	0.37	-0.31	-0.70	-0.79	-0.56
	0.39	-0.26	0.09	-0.15	-0.15	-0.03	-0.22
	0.89	-1.12	-0.69	0.09	0.33	0.19	-0.42
	1.89	-5.81	-3.21	-0.61	-0.10	0.03	0.57

Table 12: Calibration errors for the Shifted, Free, Reduced Mixture, and full Mixture SABR models (computed as *calibrated vol* − *input vol*, expressed in bps).

For better visualization, we present a graph of the RMS error for the tested models in Figure 2. We

confirm our theoretical result that CMS volatilities less that the minimum value of ~ 60 bps cannot be reached by the calibration. (The exact calibration solution does not exist.) Moreover, for *attainable* CMS volatilities, the full Mixture model performs best. (The error is less than one bp.) This behavior is due to a certain rigidity of the volatility curves of the Shifted, Free, and Reduced Mixture models, while the full Mixture model has enough degrees of freedom to maintain the calibrated swaption volatilities with almost independent movement of the wings for the CMS volatility calibration.

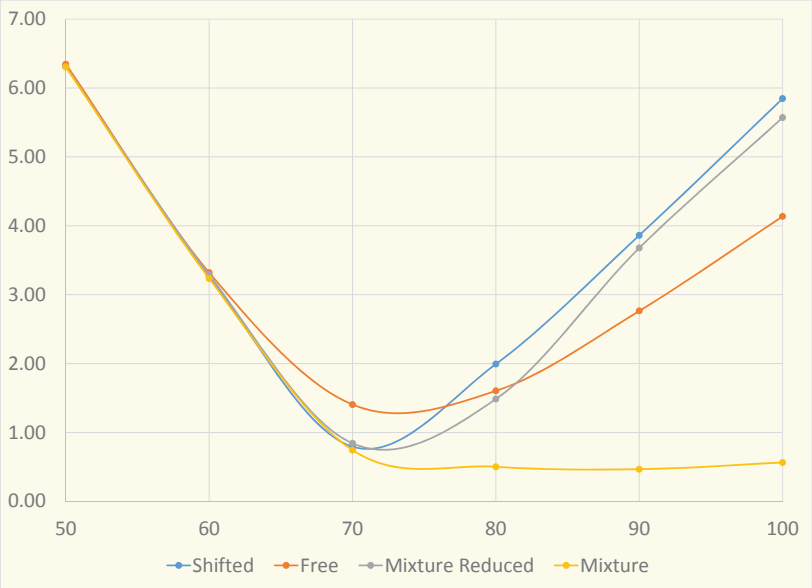

Figure 2: RMS error for the Shifted, Free, Reduced Mixture, and (full) Mixture SABR models.

Below, we present the smiles of our models with the following correspondence of Series-CMS volatility:

Series number	1	2	3	4
Input CMS vol	70	80	90	100

We do not plot the calibrated volatilities for 50 and 60 bps of the CMS volatility as it is not compatible with the option volatility input. Instead, we concentrate on the larger CMS volatilities and examine how the model does the joint calibration by the smile deformation. Figures 3–6 show the calibrated volatilities for each of the SABR models.

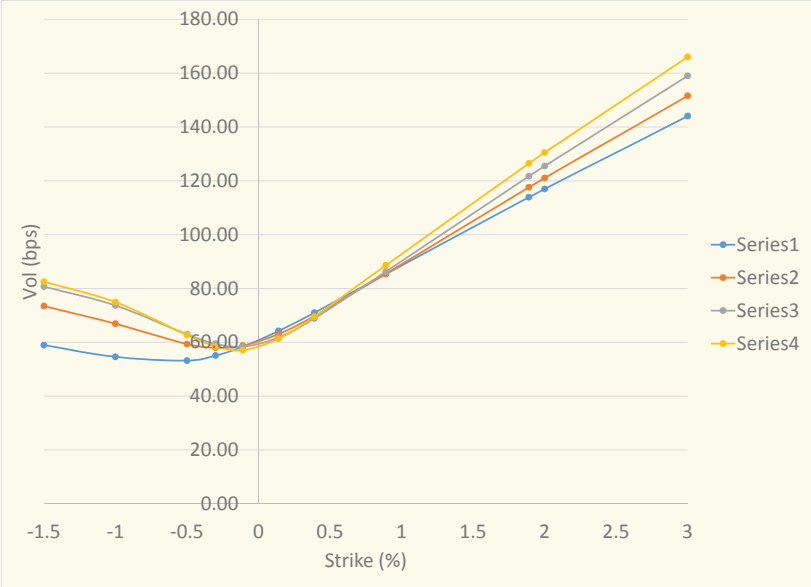

Figure 3: Calibrated Shifted SABR normal implied volatility.

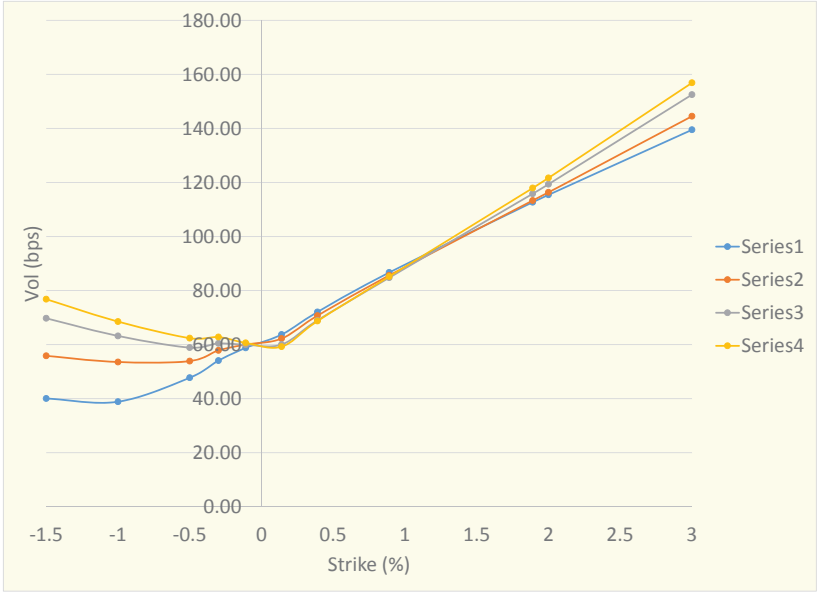

Figure 4: Calibrated Free SABR normal implied volatility.

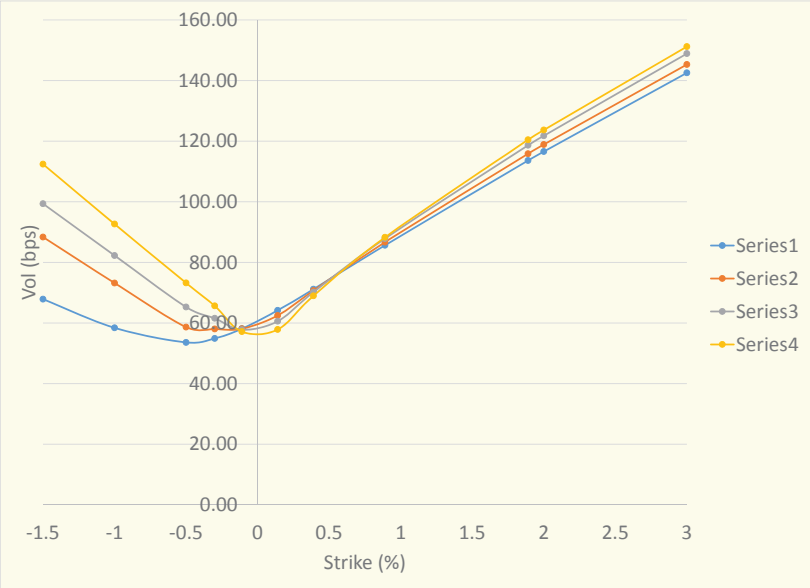

Figure 5: Calibrated Reduced Mixture SABR normal implied volatility.

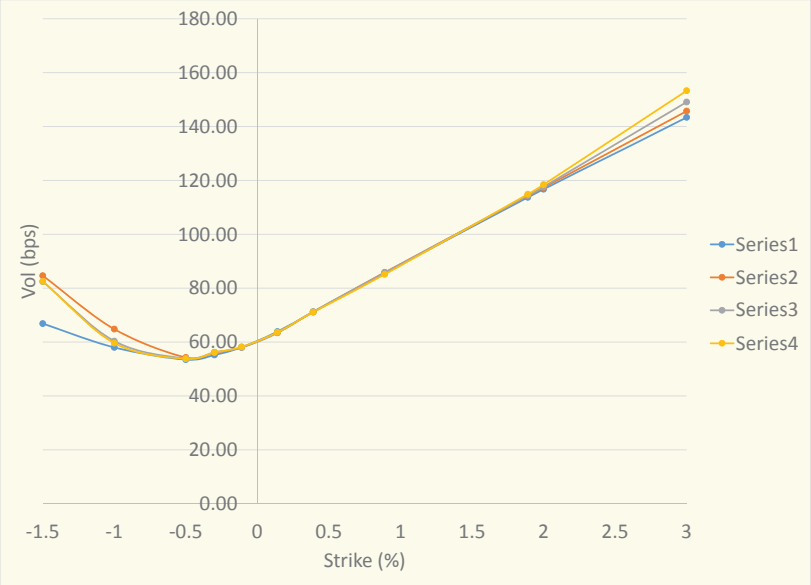

Figure 6: Calibrated Mixture SABR normal implied volatility.

We observe that only the full Mixture model is flexible enough to keep the option volatilities while

adjusting the wings to address the changing CMS volatility. The other models do not have such flexibility and deform the option volatilities away from the target.

In Figure 7, we include extreme strikes for the full Mixture model and observe the detachment of the wings from the fixed calibrated strikes.

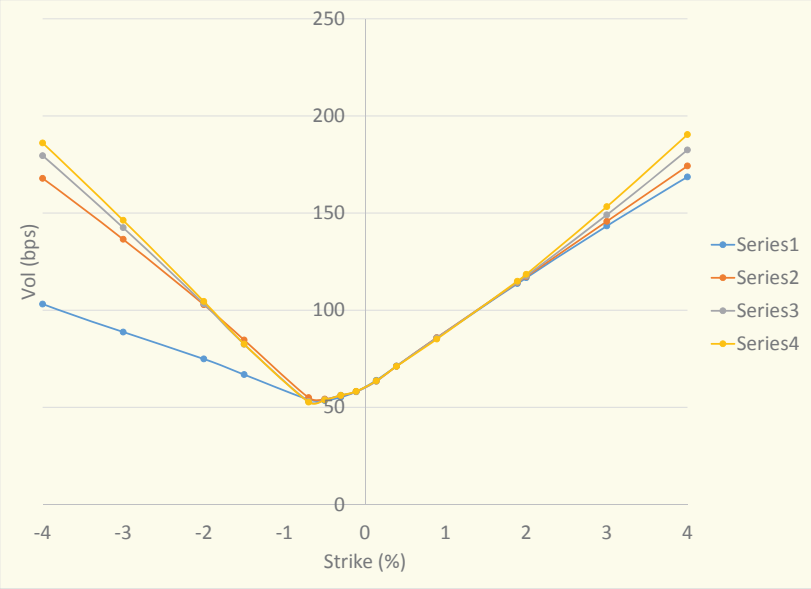

Figure 7: Calibrated Mixture SABR normal implied volatility for a large range of strikes.

8 Conclusion

We have presented here a new option pricing formula for the Normal Free SABR model that we used to improve the accuracy of our previous Free SABR model in the tails of the distribution. We also introduced a new Mixture SABR model which is arbitrage-free, allows negative rates, and has a closed form solution for option prices. In addition, the added degrees of freedom allow this model to calibrate to a larger number of swaptions as well as to combinations of swaptions and a single CMS payment.

The authors are indebted to their colleagues at Numerix, especially to Gregory Whitten and Serguei Issakov for supporting this work and Nic Trainor for the excellent editing.

A Derivation of the normal SABR option price

For $\beta = 0$, the driving SDEs are

$$dF_t = V_t \; dW_{1,t},$$
$$dV_t = V_t \; dW_{2,t},$$

with $\mathbb{E}(dW_1 dW_2) = \rho dt$. We start with the forward Kolmogorov equation for the probability density function $p(F, V)$,

$$\partial_t p(F,V) = \frac{1}{2}\left(\partial_F^2 + 2\rho\partial_F\partial_V + \partial_V^2\right) V^2 p(F,V), \tag{23}$$

and integrate over the full space (F, V) with the payoff $(F-K)^+$. In the right-hand side, only the first term (with ∂_F^2) contributes. We integrate this term by parts twice with respect to F to get the time derivative of the option in the form

$$\partial_t C(t,K) = \frac{1}{2}\int_0^\infty V^2 p(K,V) dV. \tag{24}$$

The density $p(F, V)$ proves to be proportional to the McKean heat kernel $G_{\mathrm{MK}}(t, s)$ [9] (displayed in (30) below). To show this, we note first that the geometric structure is brought into the space of state variables ($x^1 = F$, $x^2 = V$) by identifying the upper (contravariant) metric tensor with the variance matrix in the Kolmogorov equation:

$$g^{ij} = V^2 \begin{pmatrix} 1 & \rho \\ \rho & 1 \end{pmatrix}.$$

Accordingly, the lower (covariant) metric tensor g_{ij}, which is inverse to g^{ij}, determines the length element $\delta l^2 = g_{ij} dx^i dx^j$, and the determinant

$$g = \det g_{ij} = (\det g^{ij})^{-1} = V^{-4}\bar{\rho}^{-2}$$

determines the invariant, or Riemannian, volume element

$$dV_{\mathrm{inv}} = \sqrt{g} dx^1 dx^2 = V^{-2}\bar{\rho}^{-1} dF dV.$$

(We have used the notation $\bar{\rho} = \sqrt{1-\rho^2}$.) The invariant probability density (with respect to dV_{inv}), defined as

$$p_{\mathrm{inv}} = \frac{p}{\sqrt{g}} = V^2\bar{\rho}p(F,V), \tag{25}$$

satisfies the heat equation

$$\partial_t p_{\mathrm{inv}} = \frac{V^2}{2}\left(\partial_F^2 + 2\rho\partial_F\partial_V + \partial_V^2\right) p_{inv} = \frac{1}{2}\Delta p_{\mathrm{inv}}, \tag{26}$$

where

$$\Delta = \frac{1}{\sqrt{g}}\partial_i \sqrt{g} g^{ij} \partial_j \tag{27}$$

is the Laplace-Beltrami operator in the metric just defined.[3] The initial distribution of p_{inv} is the invariant delta function

$$\delta_{\mathrm{inv}}(z, z_0) = \frac{1}{\sqrt{g}}\delta(z - z_0) = V_0^2\bar{\rho}\ \delta(F - F_0)\delta(V - V_0).$$

[3]It is due to specifics of the normal SABR model and to the spacial dimension (two) that the diffusion operator in the Kolmogorov equation coincides with Laplacian. In the general SABR case, it contains additional terms called connections and charge [13].

Using the invariant density and volume has the advantage that they are true scalars that maintain their value under any change of variables. In particular, p_{inv} need only be expressed in terms of new variables with no Jacobian of transform involved.

Apply now the "diagonalizing" transform [13]

$$x = \frac{F - \rho V}{\bar{\rho}}, \qquad y = V. \tag{28}$$

In terms of the new variables x and y, the equation (26) transforms into the heat equation on the Poincaré half-plane H^2:

$$\partial_t p_{\text{inv}} = \frac{1}{2} y^2 (\partial_x^2 + \partial_y^2) p_{\text{inv}}. \tag{29}$$

For the free-boundary Normal SABR, with allows negative values of F (accordingly of x), diffusion spreads across the entire half-plane $y \geq 0$. The solution is known to be the McKean heat kernel [9]

$$p_{\text{inv}} = G_{\text{MK}}(t, s) = \frac{\sqrt{2} e^{-t/8}}{(2\pi t)^{3/2}} \int_s^\infty \frac{u\, e^{-\frac{u^2}{2t}}}{\sqrt{\cosh u - \cosh s}} du, \tag{30}$$

which depends only on time and the hyperbolic distance s in H^2, which is defined by

$$\cosh s = \frac{(x - x_0)^2 + y^2 + y_0^2}{2 y y_0}. \tag{31}$$

The function $G_{\text{MK}}(t, s)$ solves (29), where the Laplacian only contains derivatives on s because G_{MK} depends on x and y through s only:

$$\partial_t G_{\text{MK}}(t, s) = \frac{1}{2} \frac{1}{\sinh s} \partial_s \sinh s \; \partial_s G_{\text{MK}}(t, s). \tag{32}$$

The corresponding cumulative probability function $G(t, s)$, i.e., the probability to find a "particle" at a distance larger than some s, has been introduced in [2] and is calculated as

$$\begin{aligned} P(s(x, y) > s) = G(t, s) &= 2\pi \int_s^\infty G_{\text{MK}}(t, s') \sinh s' ds' \\ &= \frac{2 e^{-t/8}}{t\sqrt{\pi t}} \int_s^\infty du \sqrt{\cosh u - \cosh s}\, u\, e^{-\frac{u^2}{2t}}. \end{aligned} \tag{33}$$

The function G is properly normalized, so $G(t, 0) = 1$. Integrating equation (32) against $2\pi \sinh s$ gives

$$\partial_t G(t, s) = -\pi \sinh s \; \partial_s G_{\text{MK}}(t, s), \tag{34}$$

which is instrumental in calculating the option value.

The option time derivative (24) can be expressed through G_{MK} as

$$\partial_t C(t, K) = \frac{1}{2\bar{\rho}} \int_0^\infty G_{\text{MK}}(t, s(K, V)) dV. \tag{35}$$

The distance s is defined by (31) with "orthogonal" coordinates x, y related to the original coordinates F, V through (28) and is taken at $F = K$. The last integral can be transformed by integration by parts

and by passing to s as a variable of integration. First, express $\cosh s$ (given by (31)) in terms of $F = K$ and V:

$$\cosh s = \frac{1}{2VV_0 \cosh s}\left[\frac{1}{\bar{\rho}^2}(K - \rho V - F_0 + \rho V_0)^2 + V^2 + V_0^2\right].$$

Define the scaled strike k by

$$k = \frac{K - F_0}{V_0} + \rho, \tag{36}$$

and expand $\cosh s$ in powers of V to obtain

$$\cosh s = \frac{1}{\bar{\rho}^2}\left(\frac{(k^2 + \bar{\rho}^2)V_0}{2V} + \frac{V}{2V_0} - \rho k\right). \tag{37}$$

Next, parameterize V as

$$V = V_0\sqrt{k^2 + \bar{\rho}^2}e^w,$$

giving

$$\cosh s = \frac{1}{\bar{\rho}^2}\left(\sqrt{k^2 + \bar{\rho}^2}\cosh w - \rho k\right), \tag{38}$$

so $\cosh s$ is an invertible function of w. (Note that s is positive while w may take both signs.) Adopting w as a new variable of integration, we get

$$\partial_t C(t,K) = \frac{V_0\sqrt{k^2 + \bar{\rho}^2}}{2\bar{\rho}}\int_{-\infty}^{\infty} dw\ e^w G_{\mathrm{MK}}(t, s(w)).$$

Taking into account that s is an even function of w, we keep only the even part in the exponential $e^w \to \cosh w$, then present the above integral as $\int_{-\infty}^{\infty} dw(...) = 2\int_0^{\infty} dw(...)$ and integrate by parts to obtain

$$2\int_0^{\infty} \cosh w\ G_{\mathrm{MK}}(t, s(w))\ dw\ = -2\int_{s_0}^{\infty} \sinh w(s)\ \partial_s G_{\mathrm{MK}}(t,s)\ ds,$$

where in the last passage we have switched to s as the variable of integration. The lower limit s_0 is obtained from expression (38) for $\cosh s$ at $w = 0$:

$$\cosh s_0 = \frac{1}{\bar{\rho}^2}\left(\sqrt{k^2 + \bar{\rho}^2} - \rho k\right). \tag{39}$$

Then using relation (34) between $\partial_s G_{\mathrm{MK}}$ and $\partial_t G(t,s)$ we collect the terms to obtain

$$\partial_t C(t,K) = \frac{V_0\sqrt{k^2 + \bar{\rho}^2}}{\pi\bar{\rho}}\int_{s_0}^{\infty} \frac{\sinh w(s)}{\sinh s}\ \partial_t G(t,s)\ ds.$$

Integrating with respect to time gives the option time value

$$\begin{aligned}\mathcal{O}(t,K) &= C(t,K) - (F_0 - K)^+ \\ &= \frac{V_0\sqrt{k^2 + \bar{\rho}^2}}{\pi\bar{\rho}}\int_{s_0}^{\infty} \frac{\sinh w(s)}{\sinh s}\ G(t,s)\ ds.\end{aligned}$$

(We have taken into account that $G(0,s) = 0$, which holds because at $t = 0$ the probability density $G_{MK}(0,s)$ is delta-concentrated at $s = 0$, implying that the cumulative probability of being outside any distance $s \geq s_0 > 0$ is zero.)

Finally, express $\sinh w$ through s with the help of (38) to obtain

$$\begin{aligned}\sinh^2 w &= \frac{(\bar{\rho}^2 \cosh s + \rho k)^2 - k^2 - \rho^2}{k^2 + \bar{\rho}^2} \\ &= \frac{\bar{\rho}^2}{k^2 + \bar{\rho}^2} \left[\sinh^2 s - (k - \rho \cosh s)^2\right].\end{aligned}$$

Summarizing

The option time value for the normal SABR model with nonzero correlation and with rate F not restricted by sign is given by

$$\mathcal{O}(t,K) = \frac{V_0}{\pi} \int_{s_0}^{\infty} \frac{G(t,s)}{\sinh s} \sqrt{\sinh^2 s - (k - \rho \cosh s)^2}\, ds, \tag{40}$$

where the cumulative probability $G(t,s)$, scaled strike k, and lower limit s_0 are given by (33), (36), and (39).

Zero Correlation

When $\rho = 0$, we have $\bar{\rho} = 1$, $k = \frac{K - F_0}{V_0}$, $\cosh s_0 = \sqrt{k^2 + 1}$, and $\sinh s_0 = |k|$. Then (40) simplifies to

$$\mathcal{O}(t,K) = \frac{V_0}{\pi} \int_{s_0}^{\infty} \frac{G(t,s)}{\sinh s} \sqrt{\sinh^2 s - \sinh^2 s_0}\, ds.$$

In addition, if only positive values for F are allowed, the invariant density function is represented by the difference of the direct and reflected terms, each described by the McKean kernel G_{MK} (given by (30)):

$$p_{\mathrm{inv}} = G_{\mathrm{MK}}(t, s_d) - G_{\mathrm{MK}}(t, s_r).$$

Here s_d (direct) and s_r (reflected) are hyperbolic distances (given by (31)) from the observation point ($x = F$, $y = V$) to the source ($x_0 = F_0$, $y_0 = V_0$) and to the reflected source ($x_0 = -F_0$, $y_0 = V_0$). Since the distance s depends on x and x_0 only through $(x - x_0)^2$, i.e. $(F \pm F_0)^2$, we have $s_d = s_r$ when $F = 0$. Therefore, $p_{\mathrm{inv}} = 0$ when $F = 0$, and so p_{inv} satisfies an absorbing boundary condition. We emphasize that this construction is based on the zero-correlation case on both reflection and shift symmetries of the Kolmogorov equation with respect to F. If $\rho \neq 0$, the reflection symmetry is lost due to the presence of the mixed derivative $\partial_F \partial_V$.

Alternative expression for the option value

A somewhat different approach was employed by Henry-Labordere (HL) in [9] and then by Korn and Tang (KT) in [11]. They used the integral representation (30) for the McKean kernel $G_{\mathrm{MK}}(t,s)$ rather than treating $G_{\mathrm{MK}}(t,s)$ as a given function. The time derivative (35) is then written as the two dimensional integral

$$\partial_t C(t,K) = \frac{\sqrt{2} V_0\, e^{-t/8}}{2\bar{\rho}(2\pi t)^{3/2}} \int_0^{\infty} dv \int_{s(v)}^{\infty} \frac{u\, e^{-\frac{u^2}{2t}}}{\sqrt{\cosh u - \cosh s(v)}} du, \tag{41}$$

where $v = V/V_0$ and $\cosh s(v)$ is defined by (37). HL tried to interchange the order of integration over V and u [9]. However, he erroneously claimed that the region of integration in the u-v plane was a rectangular half-strip (which it is not) that led the author to the wrong answer. The mistake was pointed out by KT who also performed integration with respect to time, thus presenting the option value in the form of a two-dimensional integral [11].

We make further step in this direction performing integration with respect to v and presenting the option value as one-dimensional integral (different from the one in (40)). The functions involved are the normal cumulative probability

$$\Phi(x) = \frac{1}{\sqrt{2\pi}} \int_{-\infty}^{x} e^{-\frac{\xi^2}{2}} d\xi$$

and the full elliptic integral of the second kind

$$E(m) = \int_0^{\pi/2} \sqrt{1 - m \sin^2 \varphi} d\varphi, \tag{42}$$

which is a standard special function, though less common than $\Phi(x)$.

Turning to the double integral (41), notice that the domain of integration in u-v plane is defined by the condition

$$\cosh u \geq \cosh s(v).$$

According to expression (37) for $\cosh s$, the variable u has a global minimum at $u = s_0$ with $\cosh s_0$ given by (39). The above inequality can be rewritten as

$$0 \geq \cosh s(v) - \cosh u = \frac{1}{2\bar{\rho}^2 v} \left[v^2 - 2(\bar{\rho}^2 \cosh u + \rho k)v + k^2 + \bar{\rho}^2 \right].$$

If integration with respect to v is performed first, v will be confined to the interval

$$v_- \leq v \leq v_+,$$

where

$$v_\pm(u) = \bar{\rho}^2 \cosh u + \rho k \pm \bar{\rho} \sqrt{\sinh^2 u - (k - \rho \cosh u)^2} \tag{43}$$

are the roots of the quadratic polynomial in brackets above.

As a result, the integral (41) is transformed to

$$\partial_t C(t,K) = \frac{\sqrt{2} V_0 \; e^{-t/8}}{2\bar{\rho}(2\pi t)^{3/2}} \int_{s_0}^{\infty} du \; u \; e^{-\frac{u^2}{2t}} \int_{v_-}^{v_+} \frac{dv}{\sqrt{\cosh u - \cosh s(v)}}.$$

At this point HL somehow ignored the dependence on v under the square root and wrote the result of integration over v as

$$J_{(v)}^{(HL)} = \frac{v_+(u) - v_-(u)}{\sqrt{\cosh u - \cosh s_0}},$$

which of course is incorrect, as pointed out in [11].

We transform the inner integral into the standard elliptic integral (42). First, using the roots $v_\pm$, we express

$$\cosh u - \cosh s(v) = \frac{(v - v_-)(v_+ - v)}{2\bar{\rho}^2 v},$$

leading to

$$J_{(v)} = \int_{v_-(u)}^{v_+(u)} \frac{dv}{\sqrt{\cosh u - \cosh s(v)}} = \sqrt{2}\bar{\rho} \int_{v_-(u)}^{v_+(u)} \frac{\sqrt{v}\ dv}{\sqrt{(v-v_-)(v_+-v)}}. \tag{44}$$

The presence of three square roots clearly indicates that integral $J_{(v)}$ is related to elliptic functions. Indeed, by introducing a new variable of integration

$$w = \sqrt{\frac{v_+ - v}{v_+ - v_-}},$$

which ranges from $w = 1$ ($v = v_-$) to $w = 0$ ($v = v_+$), we recast $J_{(v)}$ as

$$J_{(v)} = 2\bar{\rho}\sqrt{2v_+} \int_0^1 \sqrt{\frac{1 - \frac{v_+ - v_-}{v_+} w^2}{1 - w^2}} dw.$$

The standard substitution $w = \sin\varphi$ transforms $J_{(v)}$ into the canonical form $E(m)$ from (42) with $m = \frac{v_+ - v_-}{v_+}$:

$$J_{(v)} = 2\bar{\rho}\sqrt{2v_+} E(\tfrac{v_+ - v_-}{v_+}).$$

Accordingly, the time derivative $\partial_t C(t,K)$ takes the form

$$\partial_t C(t,K) = \frac{2V_0\ e^{-t/8}}{(2\pi t)^{3/2}} \int_{s_0}^{\infty} du\ u\, e^{-\frac{u^2}{2t}} \sqrt{v_+} E(\tfrac{v_+ - v_-}{v_+}).$$

(Recall that the roots $v_\pm$ (43) are functions of u.)

The last step is integrating with respect to time, for which we change orders and integrate first in time. The option time value becomes

$$\mathcal{O}(T,K) = \frac{2V_0}{(2\pi)^{3/2}} \int_{s_0}^{\infty} du\ u \sqrt{v_+} E(\tfrac{v_+ - v_-}{v_+}) \int_0^T dt\ t^{-\frac{3}{2}}\ e^{-\frac{t}{8} - \frac{u^2}{2t}}.$$

Keeping only necessary factors, consider the time integral

$$J_{(t)} = \frac{u}{\sqrt{2\pi}} \int_0^T dt\ t^{-\frac{3}{2}}\ e^{-\frac{t}{8} - \frac{u^2}{2t}},$$

for which u can be treated as a parameter. Notice that the exponent involved can be rewritten in the two forms

$$-\frac{t}{8} - \frac{u^2}{2t} = -\frac{1}{2}\left(\frac{u}{\sqrt{t}} + \frac{\sqrt{t}}{2}\right)^2 + \frac{u}{2} = -\frac{1}{2}\left(-\frac{u}{\sqrt{t}} + \frac{\sqrt{t}}{2}\right)^2 - \frac{u}{2}.$$

Introduce two variables

$$\xi_\pm(t) = -\frac{u}{\sqrt{t}} \pm \frac{\sqrt{t}}{2},$$

each going to $-\infty$ at $t = 0$. Then two forms of the exponential become

$$-\frac{t}{8} - \frac{u^2}{2t} = -\frac{\xi_-^2(t)}{2} + \frac{u}{2} = -\frac{\xi_+^2(t)}{2} - \frac{u}{2}.$$

The power factors with the differential can then be written as

$$u\ t^{-\frac{3}{2}}\ dt = -2ud(t^{-\frac{1}{2}}) = d\xi_+ + d\xi_-,$$

so that the integral $J_{(t)}$ can be transformed into

$$J_{(t)} = \frac{e^{\frac{u}{2}}}{\sqrt{2\pi}} \int_{-\infty}^{x_-} e^{-\frac{\xi_-^2}{2}} d\xi_- + \frac{e^{-\frac{u}{2}}}{\sqrt{2\pi}} \int_{-\infty}^{x_+} e^{-\frac{\xi_+^2}{2}} d\xi_+ = e^{\frac{u}{2}} \Phi\left(x_-\right) + e^{-\frac{u}{2}} \Phi\left(x_+\right), \tag{45}$$

where $x_\pm = -\frac{u}{\sqrt{T}} \pm \frac{\sqrt{T}}{2}$. Returning to the notation $T = t$, we come up with the following alternative expression for the option time value

$$\mathcal{O}(t,K) = \frac{V_0}{\pi} \int_{s_0}^{\infty} du\ \left[e^{\frac{u}{2}} \Phi\left(-\frac{u+t/2}{\sqrt{t}}\right) + e^{-\frac{u}{2}} \Phi\left(-\frac{u-t/2}{\sqrt{t}}\right) \right] \sqrt{v_+} E(\tfrac{v_+ - v_-}{v_+}),$$

with s_0 defined by (39) and $v_\pm$ by (43).

Comparing this expression with formula (11) in [11],[4]

$$\mathcal{O} \sim \int_{b_{\min}}^{\infty} g(b) h(b) db,$$

we note that $h(b)$ in [11] is in essence our $J_{(v)}$ given in (44), which we have managed to reduce to the elliptic function $E(m)$. The function $g(b)$ is defined in [11] in a rather complicated way and can be substantially simplified. By using the complementary property of the normal cumulative probability, $\Phi(z) + \Phi(-z) = 1$, and by passing to opposite arguments in the involved probabilities $\Phi(z)$, function $g(b)$ can be expressed through

$$4\pi g(b) = e^{-\frac{b}{2}} \Phi\left(\frac{-b+T'}{\sqrt{2T'}}\right) + e^{\frac{b}{2}} \Phi\left(-\frac{b+T'}{\sqrt{2T'}}\right),$$

which is equivalent to our $J_{(t)}$ in (45).

B Calibrated model parameters

In this appendix we present the calibrated model parameters for our set of input options and a variety of the input CMS volatilities that were used for the joint calibration.

[4] We use here the authors' notations.

Input CMS vol (bps)	50	60	70	80	90	100
α	0.0258	0.0329	0.0297	0.0287	0.0365	0.0360
β	0.3847	0.4423	0.4221	0.4196	0.4842	0.4870
γ	0.5245	0.5449	0.8284	1.1262	1.4425	1.6656
ρ	0.9728	0.8571	0.3778	0.0842	-0.1532	-0.1807
shift	0.0200	0.0200	0.0200	0.0200	0.0200	0.0200

Table 13: Shifted SABR model parameters after the joint calibration.

Input CMS vol (bps)	50	60	70	80	90	100
α	0.0056	0.0058	0.0093	0.0134	0.0207	0.0285
β	0.0003	0.0017	0.0650	0.1200	0.1870	0.2323
γ	0.7147	0.7505	0.7400	0.7600	0.7800	0.7873
ρ	0.9286	0.8365	0.9000	0.7499	0.6200	0.5793

Table 14: Free SABR model parameters after the joint calibration.

Input CMS vol (bps)	50	60	70	80	90	100
α_1	0.0057	0.0057	0.0056	0.0311	0.0646	0.1176
β_1	0.0003	0.0000	0.0007	0.2481	0.3458	0.4133
γ_1	0.6762	0.7728	0.9619	0.6827	0.5699	0.4116
α_2	0.0057	0.0057	0.0055	0.0057	0.0061	0.0070
ρ_2	0.9701	0.7803	0.4891	0.9900	0.9900	0.9779
γ_2	0.6764	0.7728	0.9625	0.9081	0.8712	0.7017
p	0.0023	0.0001	0.0071	0.5900	0.6908	0.7941

Table 15: Reduced mixture SABR model parameters after the joint calibration.

Input CMS vol (bps)	50	60	70	80	90	100
α_1	0.0057	0.0060	0.0258	0.0529	0.1514	0.1684
β_1	0.0009	0.0058	0.2209	0.3255	0.4706	0.4878
γ_1	0.0094	0.0013	0.0463	0.9574	1.2370	1.6780
α_2	0.0057	0.0058	0.0057	0.0058	0.0061	0.0061
ρ_2	0.9896	0.8866	0.6917	0.9776	0.9815	0.9900
γ_2	0.6689	0.7707	0.9452	0.5926	0.5479	0.5044
p	0.0058	0.1243	0.2383	0.2469	0.1701	0.1372

Table 16: Mixture SABR model parameters after the joint calibration.

References

[1] Andreasen J. and Huge B. (2013) "Expanded Forward Volatility", RISK magazine, January

[2] Antonov A., Konikov M. and Spector M. (2013) "SABR spreads its wings", RISK magazine, August

[3] Antonov A., Konikov M., Rufino D. and Spector M. (2014) "Exact Solution to CEV Model with Uncorrelated Stochastic Volatility", SSRN paper

[4] Antonov A., Konikov M. and Spector M. (2015) "The Free Boundary SABR: Natural Extension to Negative Rates", SSRN paper

[5] Balland P. and Tran Q. (2013) "SABR goes normal", Risk magazine, May

[6] Hagan P., Kumar D., Lesnievski A., and Woodward D., (2002) "Managing Smile Risk", Wilmott Magazine, September

[7] Hagan P., Kumar D., Lesnievski A., and Woodward D., (2014) "Arbitrage Free SABR", Wilmott Magazine, January

[8] Hagan P. (2003). "Convexity Conundrums: Pricing CMS Swaps, Caps, and Floors", Wilmott magazine, March, 38–44.

[9] Henry-Labordere P., "Analysis, Geometry, and Modeling in Finance: Advanced Methods in Option Pricing", Chapman & Hall (2008).

[10] Islah O.(2009), "Solving SABR in exact form and unifying it with LIBOR market model", SSRN paper

[11] Korn R. and Tang S. (2013) "Exact Analytical Solution for the Normal SABR Model", Wilmott, v. 13, pp. 64-69

[12] Mercurio F. and Morini M. (2009) "Joining the SABR and Libor models together", Risk March, 80-85.

[13] Paulot L.(2009) "Asymptotic Implied Volatility at the Second Order with Application to the SABR Model", SSRN paper

[14] Rebonato R., McKay K. and White R. (2009) "The SABR/LIBOR Market Model: Pricing, Calibration and Hedging for Complex Interest-Rate Derivatives", John Wiley & Sons Ltd